

Electronic structure of MnO

J. van Elp, R. H. Potze, H. Eskes, R. Berger,* and G. A. Sawatzky

Department of Applied and Solid State Physics, Materials Science Centre, University of Groningen, Nijenborgh 18, NL 9747AG Groningen, The Netherlands

(Received 23 January 1991)

The electronic structure of MnO has been investigated using high-energy (x-ray photoelectron and bremsstrahlung-isochromat) spectroscopies. An experimental gap of 3.9 eV is found. By comparing the experimental results to a configuration-interaction cluster model, values for the different parameters in a model Hamiltonian are found [$U=8.5$ eV, $\Delta=8.8$ eV, and $(pd\sigma)=1.3$ eV]. These parameter values place MnO in the intermediate region of the Zaanen-Sawatzky-Allen phase diagram. By using the same parameters, the $d-d$ forbidden optical-absorption energies can be calculated, and good agreement with experiment is found.

INTRODUCTION

MnO takes a special place among the $3d$ transition-metal monoxides with the rock-salt structure because Mn^{2+} as a high-spin ion has five spin-parallel $3d$ electrons, so that the spin subbands are either completely full or completely empty. Because of this, spin-density-functional band-structure calculations predict correctly the insulating character of MnO (Refs. 1–4) in the magnetically ordered phase with a gap as large as 2.2 eV.^{3,4} Although this gap is still smaller than the gap of 3.8 to 4.2 eV,⁵ as measured with a photoconductivity experiment it is much more satisfactory than the situation in CoO for which no gap is obtained even with orbital polarization.⁶ In a band-structure calculation, the long-range magnetic order in MnO is responsible for the gap as demonstrated by Terakura *et al.*¹ who find a metallic system for the paramagnetic phase.

In all of these calculations the first electron removal states in MnO are of primarily Mn $3d$ character, which is quite different from estimates made using cluster-type calculations and atomic trends.^{7,8} From these estimates MnO falls in the intermediate region of the Zaanen-Sawatzky-Allen (ZSA) phase diagram⁹ with U (the $d-d$ Coulomb interaction) and Δ (the charge-transfer energy) almost equal and both very large. That both U and Δ are abnormally large is because of the extra stabilization of the d^5 high spin configuration by Hund's-rule coupling. According to ZSA (Ref. 9) the first ionization state should be an almost equal mixture of O $2p$ and Mn $3d$ states for $U \sim \Delta$.

That the nature of the first ionization states is expected to be quite different from the spin-density-functional band theory predictions is also strongly suggested by Svane and Gunnarsson.¹⁰ They found that by including a self-interaction correction in the band-structure calculation the gap increases to 3.98 eV for MnO and 2.59 eV for NiO, and, even more important, the $3d$ states move into or even cross the O $2p$ band. The first ionization states therefore are also found to be of highly mixed character, similar to the conclusions reached from cluster calculations.

Because of the importance of the transition-metal

monoxides as model systems to study electron correlation effects we felt that a combined study of the valence and conduction bands with x-ray photoemission spectroscopy (XPS) and inverse photoemission spectroscopy [bremsstrahlung-isochromat spectroscopy (BIS)] was warranted. In this paper we present such a study, together with a detailed analysis in terms of a configuration-interaction cluster-model calculation. In addition, we calculate the optical $d-d$ transition with the parameters obtained from a fit to the XPS and BIS measurements and find good agreement with experiment. A similar calculation, but limited to the valence-band spectrum, has recently been published by Fujimori and co-workers,^{11,12} whose conclusions were similar in some regards. We find that MnO is in the intermediate regime of the ZSA (Ref. 9) phase diagram and, because of the large values found for both U and Δ , MnO is a highly correlated insulator with a gap of 3.9 eV.

EXPERIMENTAL DETAILS AND SAMPLE PREPARATION

The XPS measurements were performed using a commercial available "top hat" X-Probe 300 from Surface Science Instruments. The x-ray source is a monochromatized Al $K\alpha$ (1486.6 eV) line. The background pressure is in the low 10^{-10} -mbar range and the used experimental resolution is 0.9 eV. The BIS experiments and the measurement of the gap were performed using a modified Kratos 200 spectrometer, with a background pressure in the low 10^{-10} -mbar range. For BIS we use an Al $K\alpha$ (1486.6-eV) monochromator for phonon detection and a home-built type of Pierce electron gun, capable of giving electron currents of approximately 100 μ A. The instrumental broadening is estimated to be 0.8 eV for BIS. BIS measurements can be severely plagued by charging effects because the electron current is quite high as compared to XPS. To overcome the charging effects encountered, we used a 1 at. % Li-doped MnO sample. The 1 at. % doping increases the conductivity considerably,¹³ and by heating the sample up to 300°C the charging effects in BIS could be overcome. The Li doping has, besides the

increased conductivity, little effect on the XPS and BIS measurements. The Li 1s core level is outside the valence-band region, and the cross-section ratio of Mn 3d compared to Li 2s is ~ 162 ,¹⁴ so that in the BIS experiment the Li 2s level shows negligible intensity. All the BIS measurements reported here were taken in several scans, which were added afterwards. The samples were checked before and after the BIS measurements with XPS. For this we used an unmonochromatized Al K α x-ray source on the Kratos 200 spectrometer, which was also used in measuring the gap. All the ceramics measured were scraped *in situ* with a diamond file.

MnO with 1% Li was prepared by the mixing in of the proper amount of Li₂MnO₃ in MnO. The stoichiometric MnO was prepared by a slowly increased heating of MnCO₃ in a H₂ atmosphere. The Li₂MnO₃ was prepared by heating the proper proportions of Li₂CO₃ and Mn₃O₄ in oxygen. In the reaction between MnO and Li₂MnO₃ care must be taken to sustain an oxygen-free atmosphere; otherwise, the reaction to higher manganese oxides (Mn₃O₄) will dominate. All the phases and transformations were checked by x-ray diffraction. The x-ray-diffraction data showed a homogeneous material with a lattice parameter of $a = 4.4415$ Å. This is slightly smaller than the lattice parameter of stoichiometric MnO ($a = 4.4450$ Å) (Ref. 15) and is the effect of the small amount of Li doping. The lattice parameter change is consistent with the lattice parameter change upon Li doping.¹⁵ The final sample is black and, on scraping, mechanically hard.

RESULTS AND DISCUSSION

Core lines

The O 1s core line in Fig. 1 shows a single line with a slight shoulder at high binding energy. This small should-

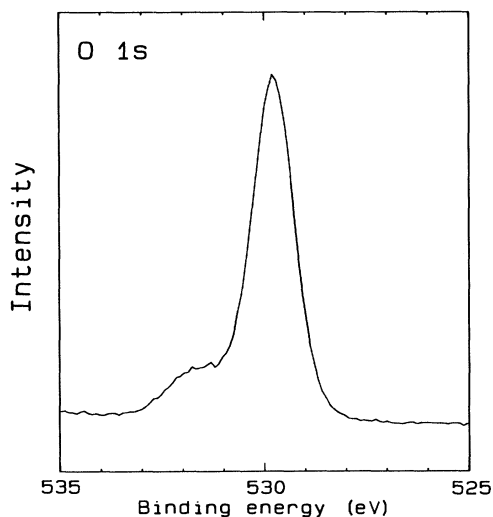


FIG. 1. Oxygen 1s core spectrum of 1 at. % Li-doped MnO. The shoulder observed at high binding energy (532 eV) is most likely due to a small amount of water, hydroxide, or defect structure present at the grain boundaries. The energy zero is the Fermi level.

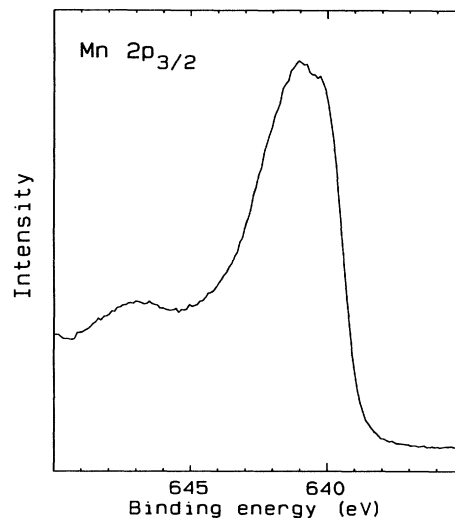


FIG. 2. Mn 2p_{3/2} core spectrum of 1 at. % Li-doped MnO. The energy zero is the Fermi level.

der is probably due to some absorbed water or defect structure at the grain boundaries. The Mn 2p_{3/2} core line in Fig. 2 shows a satellite structure at about 6 eV higher binding energy. These high-binding-energy satellites are also observed in the other late transition-metal oxides CoO,^{16,17} NiO,¹⁸ and CuO,¹⁹ and also in the manganese dihalides.²⁰⁻²² The higher-oxidation-state manganese oxides do not show these high-binding-energy satellites.^{23,24} The Mn 2p_{3/2} spectrum is comparable to the one measured by Oku, Hirokawa, and Ikeda.²³

A simple model explaining the physical origin of the high-binding-energy satellites in the core 2p_{3/2} XPS of late transition-metal oxides and dihalides is based on a cluster approach, as is shown for CuO,¹⁹ and the Cu and Ni dihalides.^{25,26} In the model the ground state is approximated by

$$\phi_g = \alpha |d^5\rangle + \beta |d^6\bar{L}\rangle + \gamma |d^7\bar{L}^2\rangle. \quad (1)$$

The \bar{L} stands for a ligand (O 2p) hole. In the final state we have a Coulomb interaction Q between the created core hole (\bar{c}) and the Mn d electrons. This pulls the $\bar{c}d^6\bar{L}$ and $\bar{c}d^7\bar{L}^2$ final states down by Q and $2Q$, respectively. As a result of this Coulomb interaction Q , the final-state levels $\bar{c}d^5$ and $\bar{c}d^6\bar{L}$ are now close together or even inverted. A similar situation occurs with the $\bar{c}d^9$ and $\bar{c}d^{10}\bar{L}$ final-state levels in CuO. In CuO (Ref. 19) the $\bar{c}d^9$ final state with its characteristic multiplet structure is clearly visible as the satellite line, and the main line is mostly $\bar{c}d^{10}\bar{L}$. The intensity of the satellite line depends very strongly on the values of the charge-transfer energy Δ , the O 2p to Mn 3d hybridization energy T , the Mott-Hubbard $d-d$ Coulomb-interaction energy U , and the core-hole 3d Coulomb interaction Q . By using a simple model with a limited number of states Oh²⁰ and Park *et al.*²¹ analyzed the manganese dihalides and found values of $U = 3.2$ eV, $T = 1.5$ eV, $Q = 4.5$ eV, and Δ , depending on the halide, between 3.2 and 9.0 eV. In their

analysis it is assumed that U , Q , and T are the same for the different dihalides. In MnO we find, after a background correction, an intensity for the first satellite line of $\sim 9\%$, and if we analyze MnO by using their Fig. 3 in Ref. 21 for Δ/T and Q/T we estimate a Δ value of around 8 eV which is very close to the value of MnF₂.

Valence and conduction band

The valence-band spectrum is similar to other XPS measurements^{11,12} and angle integrated ultraviolet photoemission spectroscopy measurements.^{27,28} The valence-band spectrum consists of the sharp peak labeled (B) (see Fig. 3) with shoulder (A) at the lower energy side, a broad structure (C), and the high-binding-energy satellite (D) at 10.5 eV. It has been claimed¹² that the high-binding-energy satellite (D) is not an intrinsic part of the MnO electronic structure, but due to defect structure, impurities, or absorbed oxygen or hydroxide. It cannot be due to a Mn₃O₄ impurity phase or defect structure at the grain boundaries because this high-binding-energy satellite is not seen in the XPS valence band of 1 at. % Li-doped Mn₃O₄.²⁴ As we will show below, we find this structure to be an intrinsic part of the 3d electron removal spectrum. This is supported by resonant photoemission experiments²⁷ in which one observes a resonance at this energy indicating Mn 3d admixture at this high binding energy. The conduction band shows a slowly rising structure attributed to the empty Mn 3d states present. The only visible effect of the 1 at. % Li doping in the conduction band could be the weak tail entering the gap as is also found in Li-doped NiO.²⁹

For determining the gap the top of the valence band is taken to be at 50% of the intensity of the shoulder labeled (A). This shoulder is more clearly visible in higher-resolution data.^{27,28} For the conduction band it is more complicated. We take the end of the gap here at 10% intensity of the rising Mn 3d structure. To this we add the energy difference of a Cu reference sample in going from 10% to 50% intensity of the Cu 4sp states. This

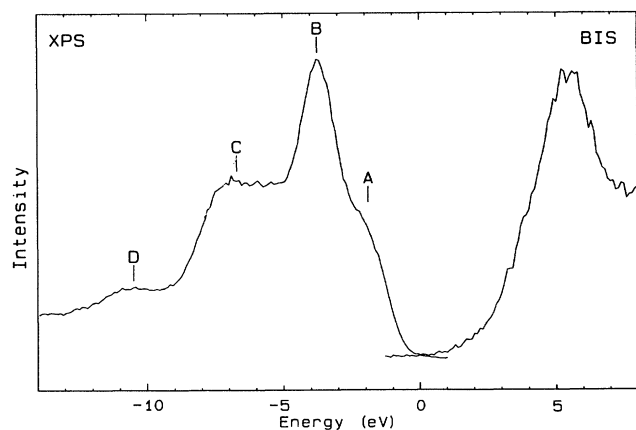


FIG. 3. XPS valence-band and BIS conduction-band measurements of 1 at. % Li-doped MnO. The energy zero is the Fermi level.

is 0.4 eV, half of the resolution of our BIS spectrometer. We ignore here the tail entering the gap. Using the above procedure we find a gap value of 3.9 ± 0.4 eV, in good agreement with a photoconductivity experiment of Drabkin *et al.*⁵ who find a gap of 3.8 to 4.2 eV.

Interpretations of valence and conduction bands

Before we discuss our own calculation we first discuss some published interpretations. One of these used by Eastman²⁸ is based on ligand field theory. The structures labeled (A) and (B) in the valence band (see Fig. 3) are ascribed to the d^4 multiplet structure in a cubic ligand field. They start from the ground $d^5(^6A_{1g})$ state obtained by filling the t_{2g} and e_g majority spin levels. Assuming that the first electron-removal state is a Mn 3d state the possible final states are $d^4\ ^5T_{2g}$ and 5E_g symmetry states as shown in Fig. 4. The splitting of these states is the combined crystal and ligand field splitting. The predicted intensity ratio 3/2 is close to what is observed for the peaks labeled (B) and (A) in Fig. 3. Such a simple pic-

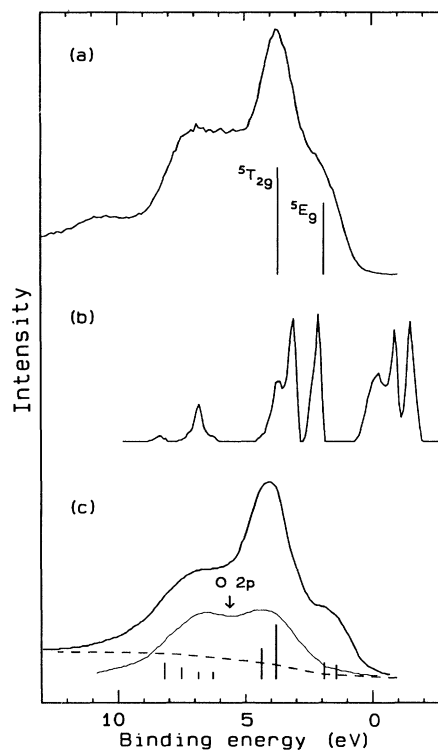


FIG. 4. (a) XPS valence-band spectrum of 1 at. % Li-doped MnO with ligand-field interpretation, the energy zero is the Fermi level; (b) band-structure calculation in the AF II ordering, the 3d partial density of states is taken from Fig. 4(a) of Ref. 1, the occupied density of states is aligned with the top of the valence band; (c) configuration-interaction cluster results of Fujimori *et al.* (Ref. 12), the O 2p spectral weight is indicated, the dashed line is a background added. The vertical bars indicate the position and intensity of the final states.

ture, however, makes it difficult to explain the broad structure (*C*) and high-binding-energy satellite (*D*). Similar to the electron-removal states, ligand field theory predicts two d^6 final states for electron addition. These are again of ${}^5T_{2g}$ and 5E_g symmetry with an intensity ratio of 3/2. In the ligand-field picture the splitting within the electron-removal and electron-addition final states should be the same and this should be equal to the ligand-field splitting in the ground-state d^5 configuration. It is quite clear that a splitting of 1.9 eV, as seen in the XPS, is too large to explain the BIS spectrum and also too large to explain the optical data in the ligand-field picture.^{30,31} This discrepancy makes clear the need for a configuration-interaction approach in which the energies of states are strongly occupation dependent.

An opposite approach to the localized ligand field description is one-electron band theory, in which each electron is assumed to occupy an itinerant Bloch state. Band-structure calculations with the actual antiferromagnetic (AF II) ordering¹⁻⁴ yield fully occupied majority-spin Mn $3d$ bands split from the empty minority-spin bands by a gap of 1.3 eV (Refs. 1 and 2), or, in a more recent calculation, 2.2 eV.^{3,4} The widths of these bands are, respectively, about 2.5 and 2.6 eV and they are split in t_{2g} and e_g character states. In the valence band the band-structure calculation can, at first sight, explain the structures labeled (*A*) and (*B*) [see Fig. 4(b)]. In the conduction band, the bandwidth is approximately the same as the width of the empty minority-spin band in the band-structure calculation. There is actually a good correspondence between the assignments made by ligand-field theory and band-structure theory. This is due to the closed-shell structure of the majority-spin d^5 Mn^{2+} ion; the multiplet structures of the allowed $d^5 \rightarrow d^4$ and $d^5 \rightarrow d^6$ transitions are identical to the occupied and unoccupied one-electron Mn $3d$ levels. The band-structure calculations cannot explain the broad valence-band structure labeled (*C*) and the high-binding-energy satellite (*D*) nor the significantly larger experimental gap measured. This is a problem also encountered in the other late transition-metal oxides.^{1,2} By including a self-interaction correction in the local-spin-density band-structure calculations a realistic value of 3.98 eV for the gap of MnO is found¹⁰ and the $3d$ states move into or even cross the O $2p$ band causing the first ionization states to be of very mixed character.

A different approach for describing the electronic structure of MnO was published by Fujimori and co-workers,^{11,12} who used a configuration-interaction calculation similar to the one we will present in the next section. We have reproduced their results in Fig. 4(c). Although their results look quite good at first sight, we have a few objections. They cannot explain the structure at 10.5-eV binding energy and they require the intensity of the oxygen $2p$ band to be three times as strong as that given by the cross-section ratio of Mn $3d$ –O $2p$.¹⁴

Configuration-interaction cluster calculation

To determine values for the various interactions involved we compare the results of the cluster calculation

with the experimental data. From the calculation we want to obtain (a) the Mn $3d$ electron-removal spectral weight, to be compared with the valence-band XPS; (b) the character (symmetry, spin, and orbital composition) of the ground state and first ionization states; (c) the Mn $3d$ electron addition spectral weight to be compared with the measured conduction band. The model calculation uses a MnO_6 cluster and a model Hamiltonian given by

$$H = H_0 + H_1, \quad (2)$$

$$H_0 = \sum_m E_d(m) d_m^\dagger d_m + \sum_m E_p(m) p_m^\dagger p_m + \sum_m T_{pd}(m) (d_m^\dagger p_m + p_m^\dagger d_m), \quad (3)$$

$$H_1 = \sum_{mm'n'} U(m, m', n, n') d_m^\dagger d_m' d_n^\dagger d_n'. \quad (4)$$

The indices m , m' , n , and n' denote orbital and spin quantum numbers. We include all the Mn $3d$ orbitals but only the oxygen orbital combinations that can hybridize with the Mn $3d$ orbitals. As a "vacuum" we take the Mn^{2+} (d^5) Hund's rule ground state (6S as a free ion, ${}^6A_{1g}$ in O_h symmetry) and a closed-shell oxygen $2p^6$. The operator d_m^\dagger creates a Mn $3d$ hole with energy $E_d(m)$. We have included a point-charge crystal-field splitting ($10Dq$), which splits the $3d$ orbitals in a double degenerate e_g hole level at $E_d(e_g) = E_d - (6Dq)$ and a triple degenerate t_{2g} level at $E_d(t_{2g}) = E_d + (4Dq)$. The value used for ($10Dq$) [$(10Dq) = 0.7$ eV] is equal to a value found in an impurity calculation³² and a cluster calculation²⁹ of the optical spectrum of NiO, which are both consistent with the experimental data. This value is also used in a similar cluster calculation of the CoO $3d$ addition spectral weight describing the conduction-band BIS experiments.¹⁷

The operator p_m^\dagger creates an oxygen $2p$ hole with energy $E_p(m)$. The ligand hole wave functions consist of linear combinations of oxygen $2p$ orbitals with the appropriate (d orbital) symmetries. The nonbonding ligand wave functions are not included. The Slater-Koster³³ oxygen nearest-neighbor interactions ($pp\sigma$) and ($pp\pi$) split the oxygen states in a double degenerate level with e_g symmetry at $E_p(e_g) = E_p + (pp\sigma - pp\pi)$ and a triple degenerate level with t_{2g} symmetry at $E_p(e_{2g}) = E_p - (pp\sigma - pp\pi)$. The value of ($pp\sigma - pp\pi$) is governed by the width of the oxygen band in MnO (~ 4 eV).²⁷

The last term of H_0 describes the one-particle hybridization between the Mn $3d$ states and the ligand orbitals. T_{pd} is the transfer integral for Mn $3d$ –O $2p$ hybridization. This is written in terms of Slater-Koster³³ ($pd\sigma$) and ($pd\pi$) transfer integrals. The transfer integral ($pd\pi$) is according to Harrison³⁴ taken to be ($pd\pi$) = $-0.45(pd\sigma)$. We define Δ as the energy needed in the ground state for removing an O $2p$ electron to the empty Mn $3d$ orbitals ($\Delta = E_p - E_d$).

H_1 describes the two-particle $3d$ Coulomb and exchange interactions U . The calculation includes the d - d Coulomb and exchange interactions using the full atomic

multiplet theory as fully specified in terms of the Racah A , B , and C parameters. For the B and C parameters the unscreened atomic values of Mn^{2+} are taken.³⁵

In this Hamiltonian we have neglected the Mn $4s, 4p$ levels and the empty O $3s, 3p$ bands. These levels are assumed to be at high energy so that their influence through hybridization can be treated as a renormalization of the effective parameters. We also neglect the O-O Coulomb interaction.

To reduce the size of the problem we omit the charge-transfer states with three ligand holes ($d^8\bar{L}^3$) or more in the calculation of the ground state (five holes) because these states are high in energy. In the electron-removal spectrum we omit in the final states for the same reason the charge-transfer states with four ligand holes or more; and in the electron-addition spectrum, the charge-transfer states with three ligand holes or more. The many-body Hamiltonian is solved exactly by means of a continued-fraction expansion of the Green's function, giving directly the electron-removal or -addition spectra.

In our calculation of the valence-band and conduction-band electronic structure we treat three parameters as free variables. These are the Racah A parameter, which is the monopole part of the $d-d$ Coulomb interaction, the on-site manganese to oxygen charge-transfer energy Δ , and the manganese oxygen charge-transfer integral ($pd\sigma$). The parameters are varied with the following criteria: (a) to reproduce in the valence band a 5E_g to ${}^5T_{2g}$ final-state splitting of 1.9 eV, to explain the experimentally observed structures (A) and (B) (Fig. 3), (b) a high-binding-energy satellite around 10.5 eV with an intensity of 10% as compared with the maximum intensity at 3.9 eV, and (c) a calculated gap of more than 5 eV to take the dispersional broadening due to translational symmetry into account.

In Fig. 5 we compare our calculated result with the experimental valence band. The broad structure (C) in the experiment is much more intense than found in the calculated $3d$ spectral weight. However, we expect oxygen-derived states at this position and should add about 18% of the $3d$ spectral weight in this region based on the cross-section ratios between Mn $3d$ and O $2p$.¹⁴ Now theory reproduces all the characteristic features of the experiment. Our parameters are listed in Table I.

In Fig. 5 we also show separately the E_g and T_{2g} symmetry final states reached by the removal of a t_{2g} or e_g $3d$ electron. The splitting of the first ionization states of the E_g and T_{2g} symmetries is equal to the ligand-field and band-structure interpretations. In addition to the 5E_g and ${}^5T_{2g}$ final states there are also 7E_g and ${}^7T_{2g}$ final states, as indicated in Fig. 5. They appear because we have $d^6\bar{L}$ states mixed in in the ground state; the transferred sixth d electron is now photoionized, leaving behind a $d^5\bar{L}$ final state with five majority spins and a parallel \bar{L} spin. This state can only hybridize with the $d^6\bar{L}^2$ final states but not with the d^4 final states. They are therefore mainly $d^5\bar{L}$ like with a small amount of $d^6\bar{L}^2$ mixed in.

In the conduction band we find two states of mainly d^6 character split by 1.0 eV into ${}^5T_{2g}$ and 5E_g symmetry states. The magnitude of the splitting of these two states

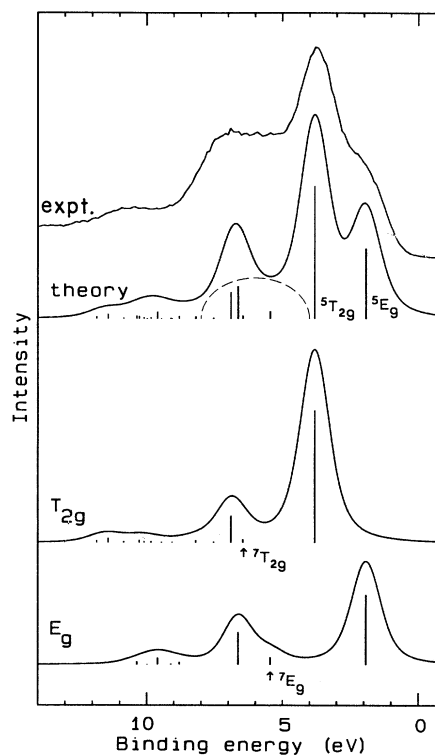


FIG. 5. The XPS valence-band spectrum (top, expt) as compared to the result of the $3d$ electron-removal spectral weight (top, theory). The vertical bars indicate the position and intensity of the final states. The dashed line indicates an oxygen band (4 eV wide) of 18% intensity as compared with the $3d$ removal spectral weight. In the bottom part we show the spectral weight for removing a t_{2g} or an e_g $3d$ electron. The energy zero is the Fermi level.

is smaller than the splitting found in the valence band. The magnitude of this splitting is mainly determined by the point-charge crystal-field parameter ($10Dq$) [$(10Dq)=0.7$ eV]. A hybridization contribution is added to this, but this added contribution is small and not very

TABLE I. Parameters used in our model Hamiltonian cluster calculation as compared to the parameters of Fujimori *et al.* (Ref. 12).

| Parameter | This work (eV) | Fujimori <i>et al.</i> (eV) |
|--|----------------|-----------------------------|
| Racah A | 3.9 | 7.3 |
| Racah B | 0.12 | 0.12–0.14 |
| Racah C | 0.41 | 0.41–0.46 |
| Δ | 8.8 | 7.0 |
| $(pd\sigma)$ | 1.3 | 0.9 |
| $(pd\pi)$ | -0.6 | -0.45 |
| $(pp\sigma)$ | -0.55 | 0 |
| $(pp\pi)$ | 0.15 | 0 |
| $(10Dq)$ | 0.7 | 0 |
| $U = A + 14B + 7C$ | 8.5 | |
| $U = A - \frac{14}{9}B + \frac{7}{9}C$ | | 7.5 |
| E_{gap} | 5.3 | |

sensitive to different parameters $[(pd\sigma), A, \Delta]$ because the d^6 final states can only hybridize with $d^7\bar{L}$ final states that are $A + \Delta$ (~ 11 eV) higher in energy. In Fig. 6 we show our calculation and the BIS spectrum. We have added a background to the calculated spectrum to describe inelastic electron-loss processes. The intensity of the background at a certain energy is proportional to the integrated intensity of the $3d$ addition spectral weight up to that energy.

Before we discuss the results we first look at the effects of different parameters. If we take $(pd\sigma) = 1.0$ eV, we find that the intensity distribution of the $3d$ removal spectral weight is still the same, but is now spread over a much smaller energy range [see Fig. 7(b)]. To spread the calculated $3d$ removal spectral weight over the measured energy range we need $(pd\sigma) = 1.3$ eV. If we change the difference between U and Δ by changing Δ with ± 1 [see Figs. 7(c) and 7(d)] we find strong changes in the intensity of the higher-binding-energy features (C) and (D). The intensity of the high-binding-energy features increases when Δ decreases, which is a result of the increase of d character in these high-binding-energy features. The first ionization states will have more $d^5\bar{L}$ character mixed in. These changes limit the difference between U and Δ considerably; we take $\Delta = 8.8 \pm 0.5$ eV. The Racah A parameter ($= 3.9$ eV) determines the value of U ($U = A + 14B + 7C = 8.5$ eV). We calculated a theoretical gap of 5.3 eV.

In comparing our results with those of Fujimori we first point out a difference in the definition of U . We have defined U in terms of the lowest Hund's rule state in each case d^{n-1} , d^n , and d^{n+1} . For Mn^{2+} , $U_{HR} = A + 14B + 7C$. Fujimori *et al.*¹² define U in terms of the multiplet average in each case $U_{av} = A - \frac{14}{9}B + \frac{7}{9}C$.

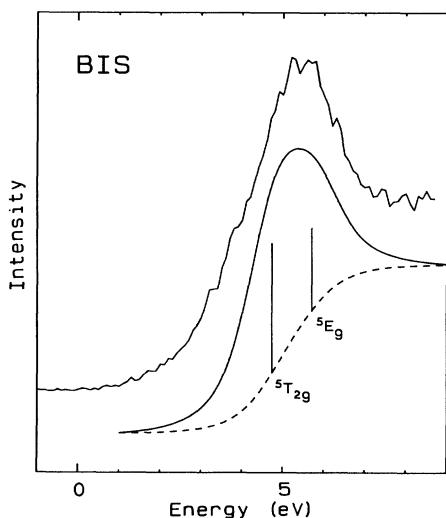


FIG. 6. The BIS valence-band spectrum (top) as compared to the electron-addition spectral weight (bottom). The dashed line is the inelastically added background as described in the text. The two different final-state symmetries are indicated. The energy zero is the Fermi level.

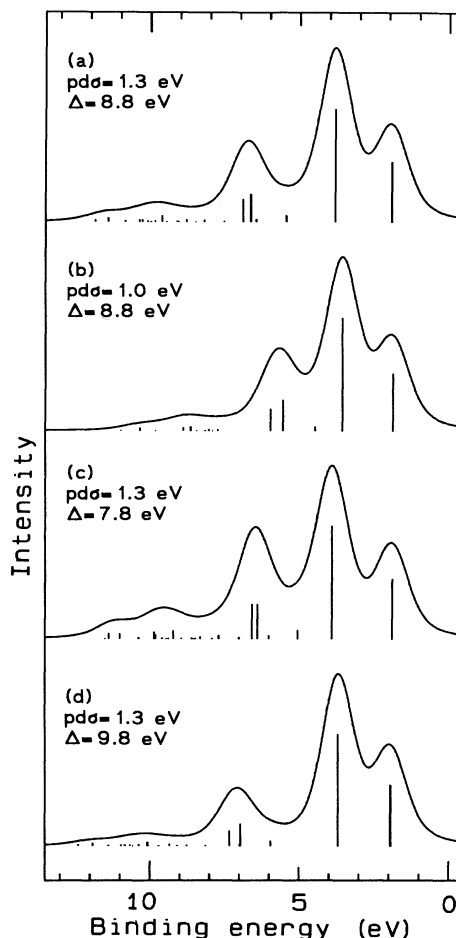


FIG. 7. The effect of different parameters on the $3d$ electron-removal spectral weight. (a) The standard parameter set of Table I. (b) $(pd\sigma) = 1.0$ eV instead of 1.3 eV. (c) $\Delta = 7.8$ eV instead of 8.8 eV. (d) $\Delta = 9.8$ eV instead of 8.8 eV.

For $B = 0.12$ and $C = 0.41$ they find $U_{av} \approx A = 7.5$ eV for Mn, $U_{HR} \approx U_{av} + 4.55$ eV. That they require such a large U value as compared to ours is at least partly due to their neglect of higher-order states. The photoemission features (A) and (B) in Fig. 3 are explained by them in a different way. The states in the shoulder [see Fig. 4(c)] are photoemission final states of mainly $d^5\bar{L}$ character and in the main peak at 3.9 eV of mainly d^4 character. The splitting in the d^6 electron addition final states is, with $10Dq = 0$ eV, around 0.2 eV, too small to explain the broad empty structures seen.

We find $U \sim \Delta$, which indicates that MnO should be placed in the intermediate region of the ZSA phase diagram.⁹ Although we find a large Δ , MnO is not completely ionic. The ground state contains 14% $d^6\bar{L}$ and 1% $d^7\bar{L}^2$ states (see Table II). The hybridization between the d^4 and $d^5\bar{L}$ final states is very strong because these states are close together ($\Delta \sim U$). This makes the first ionization states of 5E_g and $^5T_{2g}$ symmetry of very mixed character (see Table II).

TABLE II. Occupation numbers of the ground state and first two ionization states of MnO.

| Ground state ${}^6A_{1g}$ | | Ionization states | | |
|------------------------------|------|-------------------|--------------|------|
| | | 5E_g | ${}^5T_{2g}$ | |
| d^5 | 0.85 | d^4 | 0.42 | 0.52 |
| $d^6\bar{L}$ | 0.14 | $d^5\bar{L}$ | 0.50 | 0.42 |
| $d^7\bar{L}^2$ | 0.01 | $d^6\bar{L}^2$ | 0.08 | 0.06 |
| | | $d^7\bar{L}^3$ | 0.00 | 0.00 |

We can compare our parameters to the one estimated from Mn $2p_{3/2}$ core spectra and listed in the part discussing the core lines. The value for U is quite different, but this is a result of the fact that our U is defined as $d^5d^5 \rightarrow d^6d^4$ and that in the $2p$ core line U is defined as $d^6d^6 \rightarrow d^7d^5$. The difference between these two definitions is the large exchange contribution of the d^5 ion. Our Racah parameters would give for the $d^6d^6 \rightarrow d^7d^5$ a value of $U=3.0$ eV, almost the same as the value ($U=3.2$ eV) from the core line analysis. Before we compare the transfer integral T we should first define T in terms of Slater-Koster³³ parameters. For the e_g symmetry orbitals this would give $T=\sqrt{3}(pd\sigma)=2.2$ eV. The value of T tabulated by Oh²⁰ and Park *et al.*²¹ and listed is, however, a mean value between t_{2g} and e_g symmetry orbital hybridizations. The values of Δ found in both ways are quite comparable. A problem with the core line analysis is that one determines Δ by determining $\Delta-Q$ and then use $Q=4.5$ eV on the grounds of the relation $U=0.7Q$. The problem now is which definition one should take for U . It might be better to use the monopole part of the Coulomb interaction instead of U , so $A=0.7Q$. This will change the values for U , Δ , T , and Q , but not by much, because A is only slightly larger than the U used. In general, we conclude that the parameters we find in the configuration-interaction cluster model are consistent with the parameter values found from a Mn $2p_{3/2}$ core line analysis, provided the different definitions are taken into account.

Optical absorptions

Within the MnO₆ cluster we also calculated the dipole-forbidden optical intra-atomic $d-d$ transitions us-

ing the parameters obtained from the XPS-BIS experiments. We compare (see Table III) our calculated absorption energies with measured absorption energies.^{30,31} The optical-absorption spectra have in a ligand-field picture always been explained by using reduced B and C parameters. This has been explained as a result of the reduction of the $3d$ component in a molecular orbital as compared to a pure $3d$ orbital. We calculated the optical absorptions by using the same parameters as those determined from the fit on the valence- and conduction-band spectra, thereby using the free-ion Racah B and C parameters of Mn²⁺.³⁵ The calculated positions and the measured absorptions agree quite well for the first three lines and are shifted over 0.2 eV for the next two. The apparent reduction of the Racah B and C parameters mentioned above is, in the cluster configuration-interaction calculation, incorporated through the Mn $3d-O2p$ hybridization, which is symmetry dependent. The positions of the absorptions are therefore very sensitive to the Slater-Koster³³ hybridization parameters ($pd\sigma$) and ($pd\pi$). For example, as shown in Table III, some multiplets are shifted much more than others, upon switching on the hybridization. The ${}^4T_{1g}$ state originating from the 4P multiplet hardly changes because of the small effective transfer integral. The fact that we use the same value for ($pd\sigma$) as in the XPS and BIS analyses could indicate that the hybridization in the ground state is equal to the hybridization for the XPS final states.

CONCLUSIONS

We have presented experimental data on the unoccupied electronic structure of MnO. By using a combination of XPS and BIS, an experimental band gap of 3.9 ± 0.4 eV is found, in good agreement with photoconductivity experiments. The band gap is caused by strong correlation effects, which are also responsible for the breakdown of the one-electron picture. These strong correlation effects can be taken into account by using a configuration-interaction cluster model. The cluster-model calculations give with a reasonable parameter set a good representation of the experimental data. The parameters found [$\Delta=8.8$ eV, $U=8.5$ eV, and ($pd\sigma$)=1.3 eV] are consistent with parameters obtained from an analysis of the Mn $2p_{3/2}$ core lines in the dihalides and the monoxide after taking into account the different

TABLE III. The $d-d$ optical transitions of MnO calculated with the parameters of Table I and compared with the experimental values of Pratt and Coelho (Ref. 30) and Huffman, Wild, and Shinmei (Ref. 31).

| Symmetry state | Measured optical absorption | | Calculated optical absorption | |
|----------------------|-----------------------------|-----------------|-------------------------------|-----------------------------|
| | Ref. 31 (eV) | Ref. 30 (eV) | ($pd\sigma$)=1.3 eV (eV) | ($pd\sigma$)=0 eV (eV) |
| ${}^4T_{1g} ({}^4G)$ | 2.0 | 2.1 | 2.01 | 2.78 |
| ${}^4T_{2g} ({}^4G)$ | 2.6 | 2.6 | 2.56 | 3.14 |
| ${}^4A_{1g} ({}^4G)$ | 2.95 | 2.95 | 2.94 | 3.25 |
| ${}^4E_g ({}^4G)$ | 2.95 | 2.95 | 2.95 | 3.25 |
| ${}^4T_{2g} ({}^4D)$ | 3.25 | | 3.50 | 3.94 |
| ${}^4E_g ({}^4D)$ | 3.5 | | 3.69 | 4.09 |
| ${}^4T_{1g} ({}^4P)$ | | | 4.20 | 4.12 |

definitions. The high-binding-energy satellite (D) at 10.5 eV in the valence band can be very well reproduced in the cluster calculation and is not caused by impurities, defects, or contaminations, as previously proposed. We find that MnO, because U and Δ are comparable, should be placed in the intermediate region of the ZSA phase diagram. As a consequence, the first ionization states are of very mixed character. By using the parameter set found in the XPS-BIS analysis we can also predict the Mn d - d forbidden optical transitions and find good agreement with experimental d - d absorption energies.

ACKNOWLEDGMENTS

We thank A. Fujimori for helpful comments and pointing out the difference in definitions of U . This work was supported by the Netherlands Foundation for Fundamental Research on Matter (FOM), the Netherlands Foundation for Chemical Research (SON), the Netherlands Organisation for the Advancement of Pure Research (NWO), and the Committee for the European Development of Science and Technology (CODEST) program.

*Present address: Uppsala Universitet, Kemiska Institutionen, Box 531, S-75121 Uppsala, Sweden.

- ¹K. Terakura, T. Oguchi, A. R. Williams, and J. Kuebler, *Phys. Rev. B* **30**, 4734 (1984).
- ²E. J. Ojala and K. Terakura, *Phys. Rev. B* **33**, 2733 (1986).
- ³M. Belkhir and J. Hugel, *Solid State Commun.* **70**, 471 (1989).
- ⁴J. Hugel and M. Belkhir, *Z. Phys. B* **79**, 57 (1990).
- ⁵I. A. Drabkin, L. T. Emel'yanova, R. N. Iskenderov, and Y. M. Ksendzov, *Fiz. Tverd. Tela (Leningrad)* **10**, 3082 (1968) [*Sov. Phys.—Solid State* **10**, 2428 (1969)].
- ⁶M. R. Norman, *Phys. Rev. Lett.* **64**, 1162 (1990); **64**, 2466 (1990).
- ⁷J. Zaanen and G. A. Sawatzky, *J. Solid State Chem.* **88**, 8 (1990).
- ⁸J. Zaanen, Ph.D. thesis, University of Groningen, The Netherlands, 1986, Chap. 9.
- ⁹J. Zaanen, G. A. Sawatzky, and J. W. Allen, *Phys. Rev. Lett.* **55**, 418 (1985).
- ¹⁰A. Svane and O. Gunnarsson, *Phys. Rev. Lett* **65**, 1148 (1990).
- ¹¹A. Fujimori, in *Core-Level Spectroscopy in Condensed Systems*, edited by J. Kanamori and A. Kotani (Springer-Verlag, New York, 1988).
- ¹²A. Fujimori, N. Kimizuka, T. Akahane, T. Chiba, S. Kimura, F. Minami, K. Siratori, M. Taniguchi, S. Ogawa, and S. Suga, *Phys. Rev. B* **42**, 7580 (1990).
- ¹³C. Crevecoeur and H. J. de Wit, *J. Phys. Chem. Solids* **31**, 783 (1970).
- ¹⁴J. J. Yeh and I. Lindau, *At. Data Nucl. Data Tables* **32**, 1 (1985).
- ¹⁵W. D. Johnson and R. R. Heikes, *J. Am. Chem. Soc.* **78**, 3255 (1956).
- ¹⁶Z.-X. Shen, J. W. Allen, P. A. P. Lindberg, D. S. Dessau, B. O. Wells, A. Borg, W. Ellis, J. S. Kang, S. J. Oh, I. Lindau, and W. E. Spicer, *Phys. Rev. B* **42**, 1817 (1990).
- ¹⁷J. van Elp, J. L. Wieland, H. Eskes, P. Kuiper, G. A. Sawatzky, F. M. F. de Groot, M. Abbate, and T. S. Turner (unpublished).
- ¹⁸S. Hüfner and G. K. Wertheim, *Phys. Rev. B* **8**, 4857 (1973).
- ¹⁹J. Ghijsen, L. H. Tjeng, J. van Elp, H. Eskes, J. Westerink, G. A. Sawatzky, and M. T. Czyzyk, *Phys. Rev. B* **38**, 11 322 (1988).
- ²⁰S.-J. Oh, in *Core-level Spectroscopy in Condensed Systems* (Ref. 11).
- ²¹J. Park, S. Ryu, M. Han, and S.-J. Oh, *Phys. Rev. B* **37**, 10 867 (1988).
- ²²M. Okusawa, *Phys. Status Solidi B* **124**, 673 (1984).
- ²³M. Oku, K. Hirokawa, and S. Ikeda, *J. Electron Spectrosc.* **7**, 465 (1975).
- ²⁴R. H. Potze and J. van Elp, unpublished work on Li-substituted Mn oxides.
- ²⁵G. van der Laan, C. Westra, C. Haas, and G. A. Sawatzky, *Phys. Rev. B* **23**, 4369 (1981).
- ²⁶J. Zaanen, C. Westra, and G. A. Sawatzky, *Phys. Rev. B* **33**, 8060 (1986).
- ²⁷R. J. Lad and V. E. Heinrich, *Phys. Rev. B* **38**, 10 860 (1985).
- ²⁸D. E. Eastman and J. L. Freeouf, *Phys. Rev. Lett.* **34**, 395 (1975).
- ²⁹J. van Elp, H. Eskes, P. Kuiper, and G. A. Sawatzky (unpublished).
- ³⁰G. W. Pratt and R. Coelho, *Phys. Rev.* **116**, 281 (1959).
- ³¹D. R. Huffman, R. L. Wild, and M. Shinmei, *J. Chem. Phys.* **50**, 4092 (1969).
- ³²J. Zaanen, Ph.D. thesis, University of Groningen, The Netherlands, 1986, Chap. 7.
- ³³J. C. Slater and G. F. Koster, *Phys. Rev.* **94**, 1498 (1954).
- ³⁴W. A. Harrison, *Electronic Structure and the Properties of Solids* (Freeman, San Francisco, 1980).
- ³⁵J. S. Griffith, *The Theory of Transition Metal Ions* (Cambridge University Press, Cambridge, 1961).